NANO LETTERS

pubs.acs.org/NanoLett

Letter

Plasmon-Enhanced Digital Fluoroimmunoassay for Subfemtomolar Detection of Protein Biomarkers

Anushree Seth, Yuxiong Liu, Rohit Gupta, Zheyu Wang, Ekansh Mittal, Samhitha Kolla, Priya Rathi, Prashant Gupta, Bijal A. Parikh, Guy M. Genin, Sumanth Gandra, Gregory A. Storch, Jennifer A. Philips, Ige A. George,* and Srikanth Singamaneni*

Cite This: *Nano Lett.* 2024, 24, 229–237

Read Online

ACCESS | Metrics & More | Article Recommendations | Supporting Information

ABSTRACT: Rapid and accurate quantification of low-abundance protein biomarkers in biofluids can transform the diagnosis of a range of pathologies, including infectious diseases. Here, we harness ultrabright plasmonic fluors as "digital nanolabels" and demonstrate the detection and quantification of subfemtomolar concentrations of human IL-6 and SARS-CoV-2 alpha and variant proteins in clinical nasopharyngeal swab and saliva samples from COVID-19 patients. The resulting digital plasmonic fluor-linked immunosorbent assay (digital p-FLISA) enables detection of SARS-CoV-2 nucleocapsid protein, both in solution and in live virions. Digital p-FLISA outperforms the "gold standard" enzyme-linked immunosorbent assay (ELISA), having a nearly 7000-fold lower limit-of-detection, and outperforms a commercial antigen test, having over 5000-fold improvement in analytical sensitivity. Detection and quantification of very low concentrations of target proteins holds potential for early detection of pathological conditions, treatment monitoring, and personalized medicine.

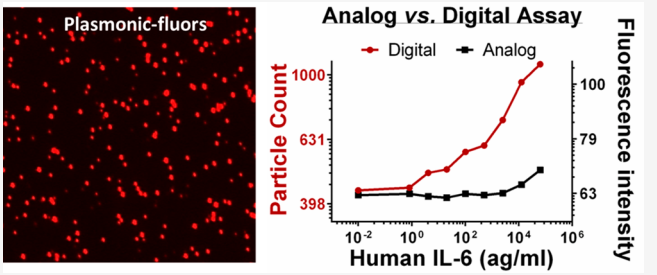

KEYWORDS: *protein detection, plasmon-enhanced fluorescence, digital immunoassay, antigen test, fluorescent nanolabels*

Ultrasensitive detection and quantification of low abundant proteins in a reliable manner is critical for early detection of pathological conditions, risk stratification and in various fields biomedical and life sciences research, including biomarker discovery and validation and drug discovery and testing.[1] To meet this need, digital immunoassays that count individual immune complexes (composed of capture antibody, analyte, and detection antibody) have been proposed. In a standard digital assay such as "single-molecule array" (SIMOA) technology, these complexes are sorted into femtoliter bins and counted,[2−4] significantly improving the limit of detection compared to their analog counterparts. However, the majority of signal is lost in the sorting process, and complex read-out procedures are required, limiting their use in routine biomedical research and clinical laboratories.[5−7]

Molecular tests that detect viral genetic material (RNA) are the current standard-of-care for identifying patients with a virus, such as severe acute respiratory syndrome coronavirus-2 (SARS-CoV-2), the virus underlying the COVID-19 pandemic. For SARS-CoV-2, reverse-transcription polymerase chain reaction (RT-PCR) is used to amplify RNA in nasopharyngeal (NP) swabs or saliva and has proven effective in tests identifying individuals who have contracted SARS-CoV-2. In the past few years, there has been remarkable progress in the detection of RNA targets in point-of-care and resource-limited settings.[8−13] Some of these methods enable naked-eye detection of RNA by harnessing the unique optical and catalytic properties nanoparticles.[8−10] However, these tests have a major shortcoming: RT-PCR testing cannot distinguish between replication-competent (infectious) virus and remnant RNA. Thus, individuals can remain positive for months after most patients cease to shed replication-competent virus.[14−19] These noninfectious individuals cannot be distinguished from infectious immunocompromised patients who shed viable SARS-CoV-2 for weeks to months.[20−23]

Antigen tests may be able to differentiate infectious individuals from those with past infections if they detect antigens that are expressed when there is a replication-competent virus, and they do not persist after viral clearance.[24,25] In the COVID-19 pandemic, accurate identification of antigen proteins from severe acute respiratory syndrome coronavirus-2 (SARS-CoV-2) within bodily fluids holds potential for reducing spread, assessing risk, and controlling emerging variants. However, existing antigen tests

Received: October 3, 2023
Revised: December 11, 2023
Accepted: December 14, 2023
Published: December 26, 2023

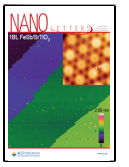

https://doi.org/10.1021/acs.nanolett.3c03789
Nano Lett. 2024, 24, 229−237

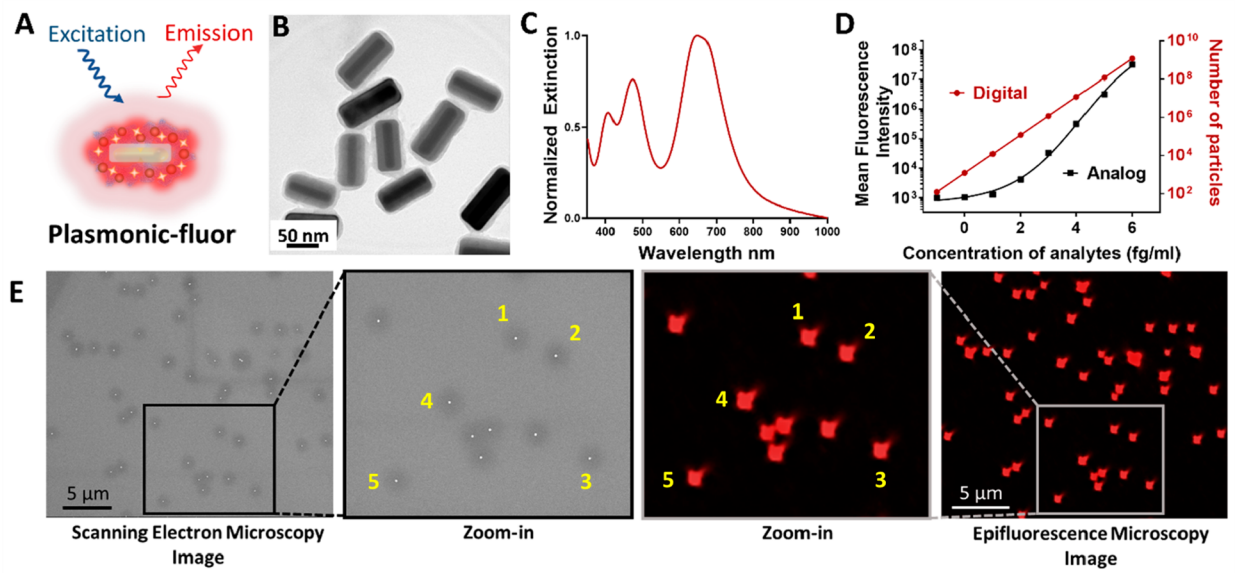

Figure 1. (A) Schematic illustration representing the design of plasmonic-fluor as a digital nanolabel. (B) Transmission electron microscopy image of PF-650. (C) Normalized visible−NIR extinction spectrum of PF-650. (D) Theoretical model comparing analog and digital p-FLISA and its effect on the slope of the standard curve at low concentration of analyte. (E) Confirmation of single particle fluorescence by correlating scanning electron microscopic images (left) and epifluorescence microscopy images (right) of the same plasmonic-fluor nanolabels. Scale bar: 5 μm.

are limited by their low accuracy and sensitivity, with a sensitivity of 37.7−84.1% compared to molecular, nucleic acid-based tests.[15,17,19,26−31]

Here, we introduce a digital protein detection technology that parallels the workflow of a standard laboratory procedure, enzyme-linked immunosorbent assay (ELISA), but improves the limit-of-detection by nearly 7000-fold. The digital detection technology relies on ultrabright fluorescent nanoconstructs, plasmonic fluors, comprising a plasmonic nanostructure (Au@Ag nanocuboid) as fluorescence enhancer, a light emitter (molecular fluorophores), and a biological recognition element (e.g., biotin, streptavidin) (Figure 1A).[32−35] Plasmonic fluors serve as digital nanolabels that can be imaged by using a standard epifluorescence microscope and counted by using a simple image-processing algorithm (Figure S1A). The system builds from partition-free bead-based assays,[36] in that it does not require sorting of the immunocomplexes into bins, but has a simple workflow analogous to that of ELISA.

DIGITAL PLASMONIC FLUOR-LINKED IMMUNOSORBENT ASSAY (DIGITAL P-FLISA)

We first established the use of plasmonic fluorescence in a "partition-free" digital assay that does not require sorting individual micro/nanoscale particles into bins prior to counting. Plasmonic fluor-IR650 (PF-650) were synthesized by coating BSA-biotin-IR650 conjugates on Au@Ag nanocuboids (Figure 1B) with a longitudinal localized surface plasmon resonance (LSPR) wavelength of 670 nm (Figure 1C). The size, shape, and composition of the plasmonic nanoantenna were chosen to maximize the plasmon-enhanced fluorescence according to our previous reports.[32,33]

We built a simple theoretical model to estimate the sensitivity of the digital plasmonic fluor-linked immunosorbent assay (p-FLISA) relative to its analogue counterpart (Figure 1D). For lower resolution (i.e., large pixel size) images, multiple labels, and consequently multiple analyte molecules, are required within one pixel to produce a discernible signal with signal-to-noise ratio (SNR) ≥ 3 (Figure S1B), thus precluding the detection of analytes at low concentrations. One-to-one correspondence between individual plasmonic-fluors in scanning electron microscopy (SEM) images and fluorescence images confirmed that the individual plasmonic fluors could be imaged with a high signal-to-background ratio (~20) (Figure S2A) using a standard epifluorescence microscope under a 20× objective (Figure 1E). In the idealized case in which each analyte molecule in a sample well is captured and labeled by a single plasmonic fluor to complete the sandwich assay, the signal intensity of the analogue assay is simply the average fluorescence signal from all pixels in an image of the well. Dose−response curves thus varied with label brightness and with spatial resolution of the image. As the brightness of the labels with respect to background pixels increased, the LOD (limit of detection, defined as the concentration of the analyte at a SNR of 3) decreased (Figure S2B). While higher resolution improves the sensitivity of the analogue assay, the finite contribution of background intensity to the mean pixel intensity still limits the LOD of the assay (Figure S2C). This limitation is mitigated in digital p-FLISA, as there is no contribution of background signal; signal intensity is determined by counting the number of the nanolabels, with the background signal below a preset threshold disregarded. Thus, the signal from the digital assay exhibits a detectable increase proportional to the analyte concentration, enabling the detection of ultralow analyte concentrations (Figure 1D). Therefore, the model suggests that the digital assay offers a broader dynamic range and lower LOD compared to analogue assay, limited only by the nonspecific binding of the detection antibodies and the nanolabels on the sensor surface.

To validate the improved bioanalytical performance (i.e., larger dynamic range and lower LOD) of the partition-free digital p-FLISA, we compared it to ELISA and analogue p-FLISA for the detection of human IL-6, a pro-inflammatory

https://doi.org/10.1021/acs.nanolett.3c03789
Nano Lett. 2024, 24, 229−237

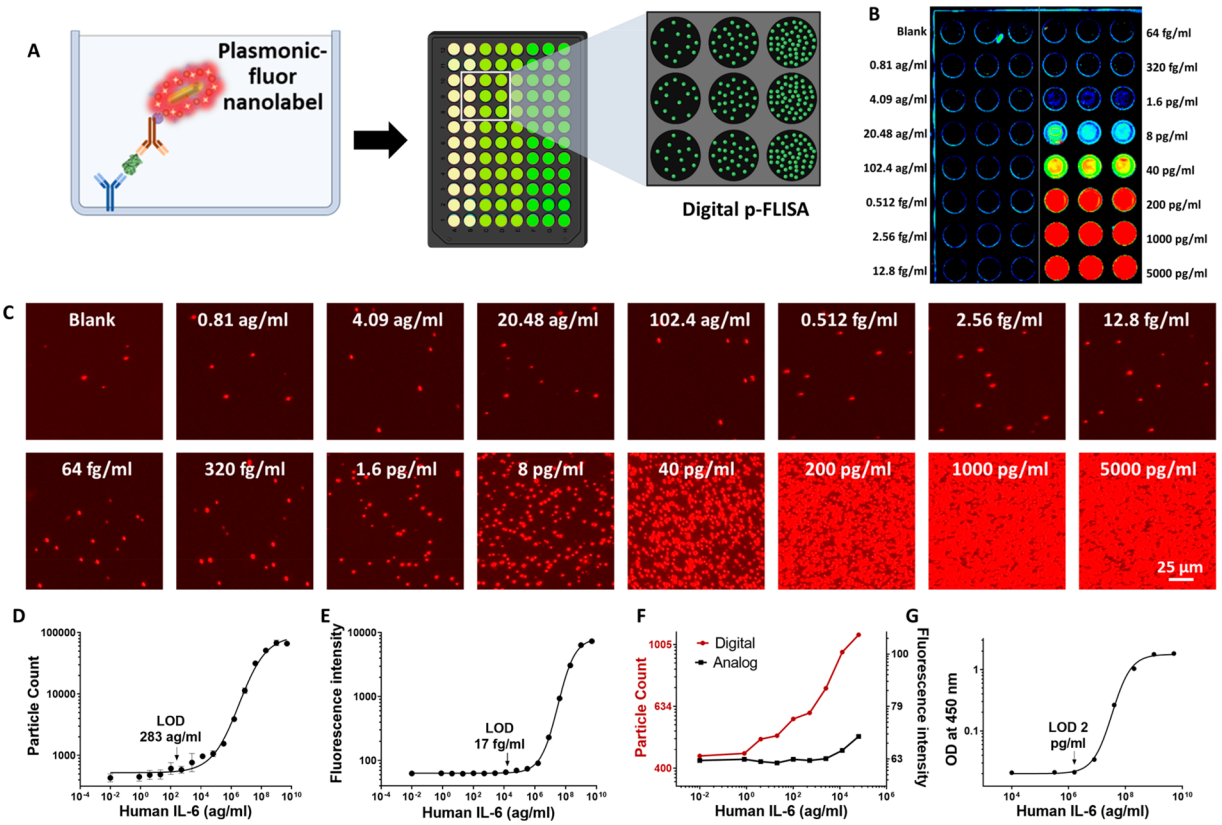

Figure 2. (A) Schematic illustration of digital p-FLISA. (B) Fluorescence image of analog p-FLISA. (C) Zoomed-in epifluorescence microscopic images of digital p-FLISA. (D) Particle count vs concentration plot of digital p-FLISA of human IL-6. $n = 2$ (5 images per well). (E) Fluorescence intensity vs concentration plot for analog p-FLISA. $n = 3$. (F) Comparison of analog vs digital. (G) ELISA ($n = 3$). Digital $R^2 = 0.9939$, Analog $R^2 = 0.9995$, ELISA $R^2 = 0.9992$.

cytokine. For the analog assays (ELISA and p-FLISA), conventional optical density or ensemble fluorescence intensity vs concentration was analyzed using a four-parameter logistic (4PL) curve to determine the LOD and limit-of-quantification (LOQ). We tested a broad range of antigen concentrations (10 log orders) 5 ng/mL to 0.81 ag/mL to determine the analytical parameters (LOD, LOQ, and dynamic range) of digital p-FLISA. The LOD was defined as the signal from the blank well plus three times the standard deviation (3σ) of the blank and was used as a parameter to compare the performance of the assays.

The digital assay protocol is essentially identical to analogue p-FLISA except that the microtiter plate is imaged using an epifluorescence microscope, and the images are analyzed using a custom-developed algorithm (Figure 2A). The number of plasmonic fluors at the bottom of the well increased monotonically with the concentration of IL-6 (Figure 2B–D). The LOD of digital p-FLISA (283 ag/mL) was over 7000-fold lower than ELISA and 60-fold lower than analogue p-FLISA (Figure 2D–G). At the lowest detectable IL-6 concentration (283 ag/mL), each microtiter well containing 200 μL of analyte solution consists ~1625 molecules. The significant improvement in sensitivity of digital p-FLISA compared to the analog counterpart stems from the ultrahigh brightness of plasmonic fluors, which enables single particle counting. Compared to analogue p-FLISA, digital p-FLISA sensitively detected changes in concentration over a broader dynamic range extending below the femtomolar concentration limit of analogue p-FLISA (Figure 2F).

We compared the performance of the plasmonic-fluor-based digital assay with that of existing fluorescent nanolabels under identical assay conditions. Specifically, we chose commercially available semiconducting quantum dots, Strep-Qdot 655 (ThermoFisher Scientific) as a fluorescent nanolabel for comparison. Under a 20× objective lens, with quantum dots as nanolabels we did not observe any discernible dose-dependence for analogue or digital assay. At higher magnification (60× objective), we observed individual particle-like features, which increased in number with an increase in the concentration of the analyte. However, these features suffered from fluorescence intermittency (blinking), making them unsuitable for digital imaging (Figure S3).[37] The LOD (~14 pg/mL) of the quantum dot-linked immunosorbent assay was nearly 1000-fold inferior compared to even analogue p-FLISA. These findings underscore the importance of ultrabright nanolabels, such as plasmonic fluors, for realizing an ultrasensitive partition-free digital detection technology, which is not feasible with moderately bright nanolabels such as quantum dots.

ULTRASENSITIVE DETECTION OF SARS-COV-2 ANTIGEN USING DIGITAL P-FLISA

Next, we set out to detect the SARS-CoV-2 specific protein antigen in human nasopharyngeal (NP) swabs and saliva (Figure 3A). Nucleocapsid (N) protein was chosen as target antigen from among the four SARS-CoV-2 structural proteins (membrane (M), envelope (E), nucleocapsid (N), and spike (S)) because of its abundance and distinct structure compared

https://doi.org/10.1021/acs.nanolett.3c03789
Nano Lett. 2024, 24, 229−237

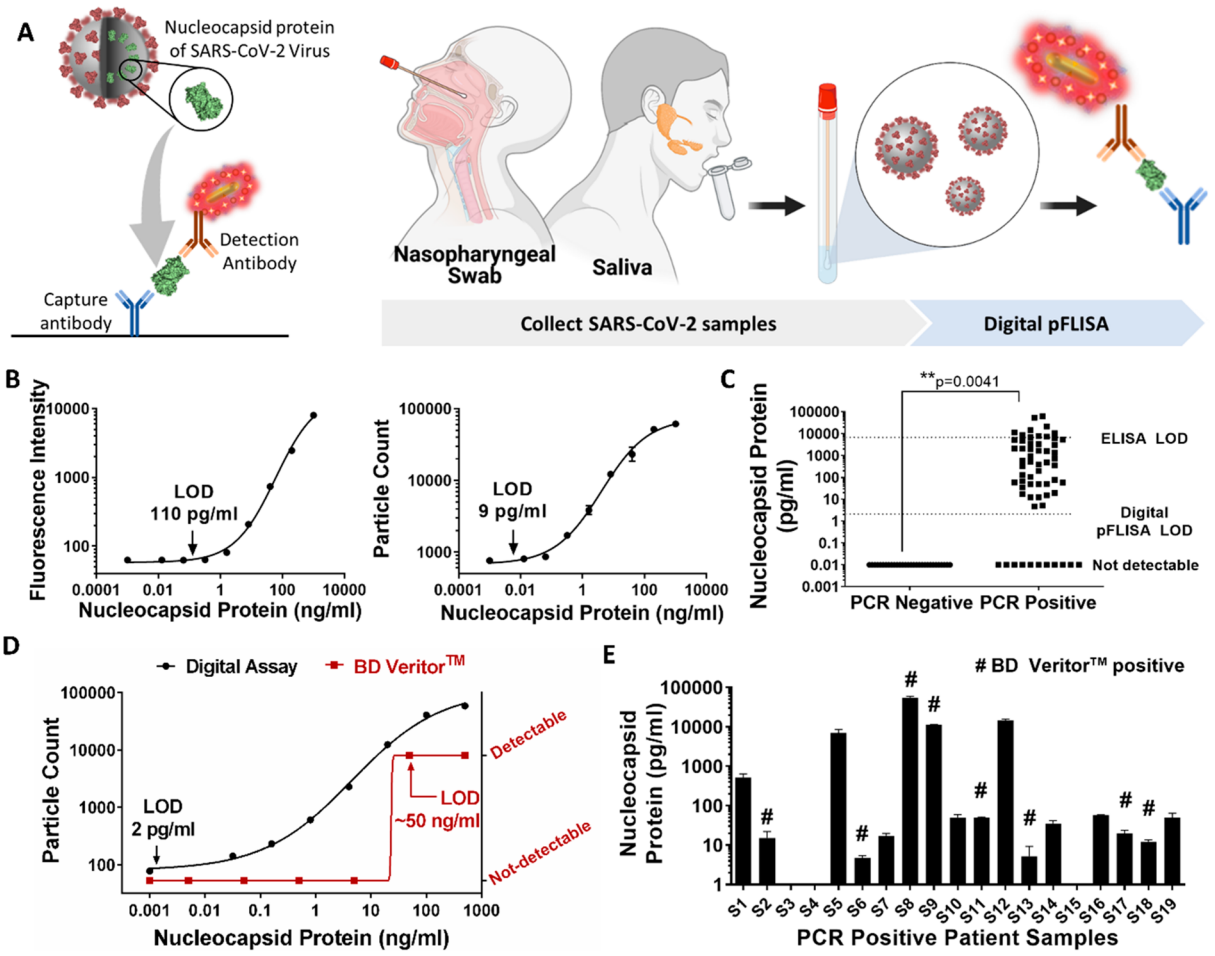

Figure 3. (A) Schematic illustration representing the collection of human nasopharyngeal (NP) swabs and saliva samples followed by digital p-FLISA. B) Fluorescence intensity vs concentration plot (analog p-FLISA) and Particle count vs concentration plot (digital p-FLISA) for detection of recombinant nucleocapsid protein. $n = 2$. (5 images per well for digital p-FLISA). Analog $R^2 = 0.9967$, Digital $R^2 = 0.9953$. (C) Concentration of nucleocapsid protein in PCR-positive ($n = 60$) and PCR-negative ($n = 30$) human swabs and saliva as calculated by digital pFLISA, $^{**}p = 0.0041$, unpaired t test (two-tailed) with Welch's correction. A low concentration (0.01 pg/mL) below the LOD was selected as an arbitrary value for representing the "not detectable" data points. (D) Comparison of the performance of a commercial antigen kit (BD Veritor) with that of a nucleocapsid protein digital assay ($n = 2$). (E) Detected nucleocapsid protein by digital assay (black bars) and BD Veritor kit (marked with #) in PCR positive patient samples ($n = 19$).

to previously reported coronaviruses. The N protein aids in transcription, replication, packaging of the viral genome. We determined the optimal concentration of capture and detection antibodies for attaining the highest sensitivity in p-FLISA. We tested nine combinations of capture and detection antibody concentrations to determine the optimal assay conditions (Figure S4, see the Materials and Methods). Under optimal assay conditions, the analogue p-FLISA exhibited a LOD of 110 pg/mL, which was further improved by digital p-FLISA to 9 pg/mL, which is 870-fold lower than ELISA (LOD of 7.9 ng/mL) (Figure 3B and Figure S5). We also verified the detection of N protein in serial dilutions of SARS-CoV-2 virus stock (diluted in UTM (BD universal viral transport media) with 0.05% Tween to disrupt the virus and release N protein). Digital p-FLISA enabled the detection of N protein in virus solutions diluted down to 100 PFU/mL compared to 1364 PFU/mL for analogue p-FLISA (Figure S6).

Finally, we set out to investigate the applicability of the digital assay in analyzing NP swabs and saliva samples obtained from 60 COVID-19 patients (RT-PCR positive) and 30 non-COVID-19 respiratory illness (RT-PCR negative) (Figure 3C). The samples were obtained from the Washington University School of Medicine's COVID-19 biorepository, and the diagnosis of SARS-CoV-2 was made based upon RT-PCR. Since NP swabs from patients are eluted in UTM, which is designed to transport and maintain the viral particles at room temperature, we first tested the performance of p-FLISA in this medium, as opposed to reagent diluent (1% BSA), described above. For the N protein digital p-FLISA, we observed a 4-fold improvement in LOD (2 pg/mL) with UTM as the standard diluent (Figure S7). Digital p-FLISA exhibited sensitivity of 82% and specificity of 100% (negative percent agreement) for N protein. The receiver operating characteristic (ROC) curve analysis for N protein showed that at a cutoff value of >2.3 pg/mL, the digital p-FLISA assay exhibited 81.6% sensitivity and 100% specificity (area under the curve (AUC) = 0.983, $p < 0.0001$) (Figure S8).

COMPARISON TO A COMMERCIAL ANTIGEN TEST

The high sensitivity of digital p-FLISA was further validated by comparison to a commercially available antigen kit with FDA emergency use authorization that had previously been

https://doi.org/10.1021/acs.nanolett.3c03789
Nano Lett. 2024, 24, 229−237

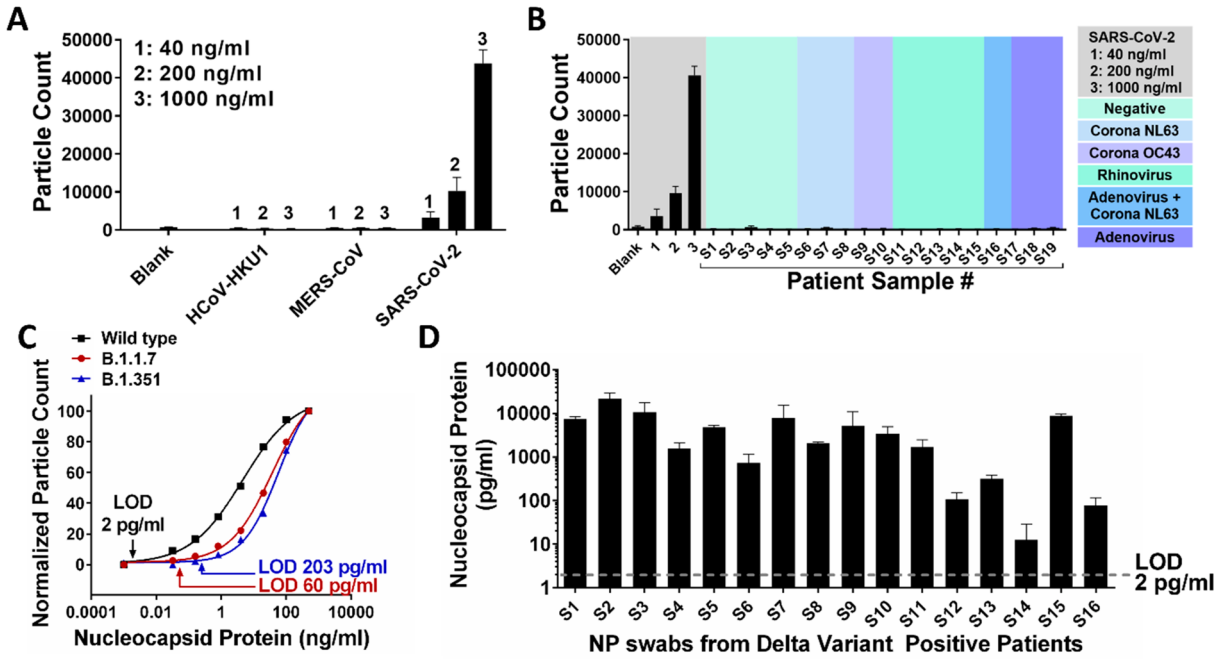

Figure 4. (A) Absence of cross-reactivity of nucleocapsid protein against recombinant protein from HCoV-HKU1 and MERS-CoV. 1:40 ng/mL, 2:200 ng/mL, 3:1000 ng/mL of N protein from different variants of viruses. (B) Particle count corresponding to concentration of nucleocapsid protein in patient samples tested positive for seasonal coronaviruses and other respiratory viruses. (C) Digital assay for nucleocapsid protein derived from SARS-CoV-2 variants B.1.1.7 (alpha) and B.1.351 (beta). (D) Concentration of nucleocapsid protein in samples positive for SARS-CoV-2 variant B.1.617.2 (delta).

validated in the Barnes Jewish Hospital clinical lab (BD Veritor, Becton, Dickinson and Company, Franklin Lakes, NJ).[38] In serial dilutions of N protein, digital p-FLISA detected concentrations down to 10 pg/mL, but the commercial antigen kit indicated samples with concentrations below 50 ng/mL as "presumptive negative," indicating that the digital p-FLISA had 5000-fold better analytical sensitivity (Figure 3D). Digital p-FLISA also outperformed the commercial antigen kit when analyzing PCR-positive COVID-19 patient samples. The commercial kit detected antigens in 8 of the 19 PCR positive samples, while the digital p-FLISA detected N protein in 16/19 (p = 0.017, using two-tailed Fisher's exact test). Among patients in the acute stage of illness (duration of symptoms <10 days), 13/14 samples tested positive by p-FLISA (93% sensitivity), compared to 7/14 by the commercial kit (50% sensitivity) (p = 0.032, using two-tailed Fisher's exact test) (Figure 3E, Table S1).

Among the remaining five, three patients were tested on day 14 of illness and two patients were asymptomatic. Among the three patients who were tested on day 14 of illness, digital p-FLISA was negative in 2 patients who had moderate COVID-19 illness and positive in one patient who had poorly controlled human immunodeficiency virus (HIV) and potentially prolonged active viral replication because of their immunocompromised status. Interestingly, this patient with poorly controlled HIV tested positive with the commercial kit and had a low RT-PCR cycle threshold (C_T) value (21.8), which supports the possibility of active viral replication. Among the two asymptomatic patients, digital p-FLISA was positive, but it is unclear whether they had active viral replication.

Although not conclusive, our results are consistent with the hypothesis that an ultrasensitive antigen test may be able to indicate current infection and possibly infectivity. Although the majority of patients (>95%) with mild to moderate COVID-19 continue to shed SARS-CoV-2 RNA from the nasopharynx for more than 10 days after symptom onset, no replication-competent virus shed beyond 9 days.[14,15] The exceptions are critically ill and immunocompromised patients, who can shed replicating virus at least through day 20.[23] Consistent with this, digital p-FLISA identified 13 out of 14 patients during the acute phase of illness when they were expected to have the replicating virus, tested negative as expected in two patients after 10 days of moderate COVID-19 illness, and tested positive as expected in an immunocompromised patient even after 10 days. These results warrant further evaluation of the p-FLISA antigen test with larger patient samples to confirm its role in identifying infectious patients as there is a need for non-culture-based tests for decision making regarding hospital infection prevention measures and removing quarantine on patients who are beyond transmissible stage of the illness. Future attempts to optimize the antigen concentration thresholds of the p-FLISA using ROC curve to accurately capture samples in the infectious stage of illness (samples with low cycle threshold (C_T) values and positive viral cultures) while retaining sufficient sensitivity may help in development of p-FLISA antigen test as a surrogate to identify replication-competent virus (Table S1).

CROSS-REACTIVITY OF N PROTEIN DIGITAL P-FLISA AND DETECTION OF SARS-COV-2 VARIANTS

Immunoassays are susceptible to cross-reactivity leading to false positive results.[39−41] The SARS-CoV-2 N protein digital assay exhibited no detectable cross-reactivity with the N protein from two other coronaviruses: MERS-CoV and HCoV-HKU1 virus (Figure 4A). The mean particle count in the blank

https://doi.org/10.1021/acs.nanolett.3c03789
Nano Lett. 2024, 24, 229−237

sample +3σ was set as the threshold for a detectable signal. Human patient NP swabs positive for other common respiratory viruses (HCoV OC43, HCoV NL63, rhinovirus, and adenovirus) exhibited no detectable signal, establishing the high specificity of digital p-FLISA for SARS-CoV-2 N proteins (Figure 4B).

Mutations in SARS-CoV-2 have led to the emergence of variants of concern that are more transmissible and with alterations to the protein or physical structure that could impact the diagnostic accuracy of antigen tests.[42,43] Most mutations in the variants of concern involve the S-gene. Although fewer N-gene mutations exist, some can escape antigen detection tests.[44,45] A diagnostic test that misses variants can potentially lead to the spread of those variants by failing to identify individuals needing isolation and hindering contact tracing efforts.

Finally, we determined the applicability of digital p-FLISA in detecting antigens from two variants of concern: B.1.1.7 (Alpha) and B.1.351 (Beta).[46] The recombinant N protein from B.1.1.7 has mutations D3L and S235F, and the recombinant protein from B.1.351 has mutation T205I. The D3L, T205I, and T205I, S235F mutations in the N protein are located outside the RNA interaction and dimer interfaces, in the intrinsically disordered regions of the N-terminal domain (NTD) and linker regions, respectively.[47] The N protein antigen corresponding to these variants was obtained from SinoBiologicals and was serially diluted, and LOD was assessed using digital p-FLISA. The N protein assay for prototypic N protein was found to be applicable to B.1.1.7 and B.1.351 variants with a LOD of 60 and 203 pg/mL, respectively (Figure 4C). We also tested 16 PCR-positive patient samples that were confirmed to be positive for B.1.617.2 (Delta) variant using gene sequencing. All samples showed a positive signal for the N protein using digital p-FLISA (Figure 4D). Thus, we conclude that digital p-FLISA holds the potential to serve as a universal method for the detection of prototypic SARS-CoV-2 as well as current and widely circulating variants.

We introduced a simple and ultrasensitive digital fluoroimmunoassay and demonstrated its utility for the detection of SARS-CoV-2 antigens. Partition-free digital p-FLISA was implemented in standard microtiter wells by using plasmonic fluors as nanolabels. These ultrabright fluorescent nanoconstructs can be imaged and counted by using a standard fluorescence microscope. The workflow for digital p-FLISA is essentially identical to that of ELISA, but digital p-FLISA exhibited a limit-of-detection that is more than 7000-fold lower than that of ELISA across multiple protein analytes. Digital p-FLISA enabled ultrasensitive detection of SARS-CoV-2 antigen and live virions through detection of N protein, with no cross-reactivity to seasonal coronaviruses and other respiratory viruses. Digital p-FLISA outperformed a commercial antigen test in terms of sensitivity and proved to be effective in detecting SARS-CoV-2 variants of concern. Results were consistent with the hypothesis that an ultrasensitive antigen test can potentially distinguish individuals with an actively replicating virus (who are thus more likely to be contagious) from patients who are past the infectious stage of illness. This simple, ultrasensitive, and widely deployable test may be useful for expanding the testing capacity and improving disease surveillance and control during infectious disease outbreaks.

■ ASSOCIATED CONTENT

Supporting Information

The Supporting Information is available free of charge at https://pubs.acs.org/doi/10.1021/acs.nanolett.3c03789.

Materials and methods, schematic illustration of the digital plasmonic-fluor-linked immunosorbent assay, additional standard curves, and patient sample information (PDF)

■ AUTHOR INFORMATION

Corresponding Authors

Ige A. George − *Division of Infectious Diseases, Department of Medicine, Washington University School of Medicine, St. Louis, Missouri 63130, United States*; Email: igegeorge@wustl.edu

Srikanth Singamaneni − *Department of Mechanical Engineering and Materials Science, Institute of Materials Science and Engineering, Washington University in St. Louis, St. Louis, Missouri 63130, United States; Siteman Cancer Center, Washington University in St. Louis, St. Louis, Missouri 63110, United States*; orcid.org/0000-0002-7203-2613; Email: singamaneni@wustl.edu

Authors

Anushree Seth − *Department of Mechanical Engineering and Materials Science, Institute of Materials Science and Engineering, Washington University in St. Louis, St. Louis, Missouri 63130, United States*; orcid.org/0000-0003-2995-2200

Yuxiong Liu − *Department of Mechanical Engineering and Materials Science, Institute of Materials Science and Engineering, Washington University in St. Louis, St. Louis, Missouri 63130, United States*

Rohit Gupta − *Department of Mechanical Engineering and Materials Science, Institute of Materials Science and Engineering, Washington University in St. Louis, St. Louis, Missouri 63130, United States*

Zheyu Wang − *Department of Mechanical Engineering and Materials Science, Institute of Materials Science and Engineering, Washington University in St. Louis, St. Louis, Missouri 63130, United States*

Ekansh Mittal − *Department of Molecular Microbiology and Division of Infectious Diseases, Department of Medicine, Washington University School of Medicine, St. Louis, Missouri 63130, United States*

Samhitha Kolla − *Department of Mechanical Engineering and Materials Science, Institute of Materials Science and Engineering, Washington University in St. Louis, St. Louis, Missouri 63130, United States*

Priya Rathi − *Department of Mechanical Engineering and Materials Science, Institute of Materials Science and Engineering, Washington University in St. Louis, St. Louis, Missouri 63130, United States*

Prashant Gupta − *Department of Mechanical Engineering and Materials Science, Institute of Materials Science and Engineering, Washington University in St. Louis, St. Louis, Missouri 63130, United States*; orcid.org/0009-0008-6291-9465

Bijal A. Parikh − *Department of Pathology and Immunology, Washington University in St. Louis, St. Louis, Missouri 63110, United States*

https://doi.org/10.1021/acs.nanolett.3c03789
Nano Lett. 2024, 24, 229−237

Guy M. Genin − *Department of Mechanical Engineering and Materials Science, Institute of Materials Science and Engineering, Washington University in St. Louis, St. Louis, Missouri 63130, United States;* orcid.org/0000-0003-3612-4729

Sumanth Gandra − *Division of Infectious Diseases, Department of Medicine, Washington University School of Medicine, St. Louis, Missouri 63130, United States*

Gregory A. Storch − *Department of Pediatrics, Washington University School of Medicine, St. Louis, Missouri 63110, United States*

Jennifer A. Philips − *Department of Molecular Microbiology and Division of Infectious Diseases, Department of Medicine, Washington University School of Medicine, St. Louis, Missouri 63130, United States*

Complete contact information is available at: https://pubs.acs.org/10.1021/acs.nanolett.3c03789

Notes

The authors declare the following competing financial interest(s): S.S. is an inventor on a provisional patent related to plasmonic-fluor technology and the technology has been licensed by the Office of Technology Management at Washington University in St. Louis to Auragent Bioscience LLC. S.S. is a co-founder/shareholder of Auragent Bioscience LLC. S.S. along with Washington University may have financial gain through Auragent Bioscience, LLC through this licensing agreement. A.S. is currently employed with Auragent Bioscience. These potential conflicts of interest have been disclosed and are being managed by Washington University in St. Louis.

■ ACKNOWLEDGMENTS

A subset of clinical samples used in this study was obtained from the Washington University School of Medicine's COVID-19 biorepository, which is supported by the Barnes-Jewish Hospital Foundation; the Siteman Cancer Center grant P30 CA091842 from the National Cancer Institute of the National Institutes of Health; and the Washington University Institute of Clinical and Translational Sciences grant UL1TR002345 from the National Center for Advancing Translational Sciences of the National Institutes of Health. This repository was developed and is maintained by Jane O'Halloran, MD, PhD; Charles Goss, PhD, and Phillip Mudd, MD, PhD, and the authors acknowledge their gratitude to them. The content is solely the responsibility of the authors and does not necessarily represent the view of the National Institutes of Health. Additional support was provided by the National Science Foundation (CBET-2224610, CBET-2316285, CMMI-1548571), National Cancer Institute-Innovative Molecular Analysis Technologies (R21CA236652 and R21CA236652-S1).

■ REFERENCES

(1) Cohen, L.; Walt, D. R. Highly Sensitive and Multiplexed Protein Measurements. *Chem. Rev.* **2019**, *119* (1), 293−321.

(2) Cohen, L.; Cui, N.; Cai, Y.; Garden, P. M.; Li, X.; Weitz, D. A.; Walt, D. R. Single Molecule Protein Detection with Attomolar Sensitivity Using Droplet Digital Enzyme-Linked Immunosorbent Assay. *ACS Nano* **2020**, *14* (8), 9491−9501.

(3) Dinh, T. L.; Ngan, K. C.; Shoemaker, C. B.; Walt, D. R. Using Antigen−antibody Binding Kinetic Parameters to Understand Single-Molecule Array Immunoassay Performance. *Anal. Chem.* **2016**, *88* (23), 11335−11339.

(4) Rissin, D. M.; Kan, C. W.; Campbell, T. G.; Howes, S. C.; Fournier, D. R.; Song, L.; Piech, T.; Patel, P. P.; Chang, L.; Rivnak, A. J.; Ferrell, E. P.; Randall, J. D.; Provuncher, G. K.; Walt, D. R.; Duffy, D. C. Single-molecule enzyme-linked immunosorbent assay detects serum proteins at subfemtomolar concentrations. *Nat. Biotechnol.* **2010**, *28* (6), 595−599.

(5) Wilson, D. H.; Rissin, D. M.; Kan, C. W.; Fournier, D. R.; Piech, T.; Campbell, T. G.; Meyer, R. E.; Fishburn, M. W.; Cabrera, C.; Patel, P. P.; Frew, E.; Chen, Y.; Chang, L.; Ferrell, E. P.; von Einem, V.; McGuigan, W.; Reinhardt, M.; Sayer, H.; Vielsack, C.; Duffy, D. C. The Simoa HD-1 Analyzer: A Novel Fully Automated Digital Immunoassay Analyzer with Single-Molecule Sensitivity and Multiplexing. *Journal of Laboratory Automation* **2016**, *21* (4), 533−547.

(6) Witters, D.; Knez, K.; Ceyssens, F.; Puers, R.; Lammertyn, J. Digital microfluidics-enabled single-molecule detection by printing and sealing single magnetic beads in femtoliter droplets. *Lab Chip* **2013**, *13* (11), 2047−2054.

(7) Decrop, D.; Brans, T.; Gijsenbergh, P.; Lu, J.; Spasic, D.; Kokalj, T.; Beunis, F.; Goos, P.; Puers, R.; Lammertyn, J. Optical Manipulation of Single Magnetic Beads in a Microwell Array on a Digital Microfluidic Chip. *Anal. Chem.* **2016**, *88* (17), 8596−8603.

(8) Moitra, P.; Alafeef, M.; Dighe, K.; Frieman, M. B.; Pan, D. Selective Naked-Eye Detection of SARS-CoV-2 Mediated by N Gene Targeted Antisense Oligonucleotide Capped Plasmonic Nanoparticles. *ACS Nano* **2020**, *14* (6), 7617−7627.

(9) Alafeef, M.; Moitra, P.; Dighe, K.; Pan, D. Hyperspectral Mapping for the Detection of SARS-CoV-2 Using Nanomolecular Probes with Yoctomole Sensitivity. *ACS Nano* **2021**, *15* (8), 13742−13758.

(10) He, M.; Xu, X.; Wang, H.; Wu, Q.; Zhang, L.; Zhou, D.; Tong, Y.; Su, X.; Liu, H. Nanozyme-Based Colorimetric SARS-CoV-2 Nucleic Acid Detection by Naked Eye. *Small* **2023**, *19* (20), No. 2208167.

(11) Rauch, J. N.; Valois, E.; Solley, S. C.; Braig, F.; Lach, R. S.; Audouard, M.; Ponce-Rojas, J. C.; Costello, M. S.; Baxter, N. J.; Kosik, K. S.; Arias, C.; Acosta-Alvear, D.; Wilson, M. Z. A Scalable, Easy-to-Deploy Protocol for Cas13-Based Detection of SARS-CoV-2 Genetic Material. *J. Clin. Microbiol.* **2021**, *59* (4), DOI: 10.1128/JCM.02402-20.

(12) Baek, Y. H.; Um, J.; Antigua, K. J. C.; Park, J.-H.; Kim, Y.; Oh, S.; Kim, Y.-i.; Choi, W.-S.; Kim, S. G.; Jeong, J. H.; Chin, B. S.; Nicolas, H. D. G.; Ahn, J.-Y.; Shin, K. S.; Choi, Y. K.; Park, J.-S.; Song, M.-S. Development of a reverse transcription-loop-mediated isothermal amplification as a rapid early-detection method for novel SARS-CoV-2. *Emerging Microbes & Infections* **2020**, *9* (1), 998−1007.

(13) Agarwal, S.; Warmt, C.; Henkel, J.; Schrick, L.; Nitsche, A.; Bier, F. F. Lateral flow−based nucleic acid detection of SARS-CoV-2 using enzymatic incorporation of biotin-labeled dUTP for POCT use. *Anal. Bioanal. Chem.* **2022**, *414* (10), 3177−3186.

(14) Owusu, D.; Pomeroy, M. A.; Lewis, N. M.; Wadhwa, A.; Yousaf, A. R.; Whitaker, B.; Dietrich, E.; Hall, A. J.; Chu, V.; Thornburg, N.; et al. Persistent SARS-CoV-2 RNA Shedding without Evidence of Infectiousness: A Cohort Study of Individuals with COVID-19. *J. Infect. Dis.* **2021**, *224* (8), 1362−1371.

(15) Wölfel, R.; Corman, V. M.; Guggemos, W.; Seilmaier, M.; Zange, S.; Müller, M. A.; Niemeyer, D.; Jones, T. C.; Vollmar, P.; Rothe, C.; Hoelscher, M.; Bleicker, T.; Brünink, S.; Schneider, J.; Ehmann, R.; Zwirglmaier, K.; Drosten, C.; Wendtner, C. Virological assessment of hospitalized patients with COVID-2019. *Nature* **2020**, *581* (7809), 465−469.

(16) Mina, M. J.; Parker, R.; Larremore, D. B. Rethinking Covid-19 Test Sensitivity — A Strategy for Containment. *New England Journal of Medicine* **2020**, *383* (22), No. e120.

(17) Bullard, J.; Dust, K.; Funk, D.; Strong, J. E.; Alexander, D.; Garnett, L.; Boodman, C.; Bello, A.; Hedley, A.; Schiffman, Z. Predicting infectious SARS-CoV-2 from diagnostic samples. *Clin Infect Dis* **2020**, *71*, 2663.

(18) He, X.; Lau, E. H. Y.; Wu, P.; Deng, X.; Wang, J.; Hao, X.; Lau, Y. C.; Wong, J. Y.; Guan, Y.; Tan, X.; Mo, X.; Chen, Y.; Liao, B.; Chen, W.; Hu, F.; Zhang, Q.; Zhong, M.; Wu, Y.; Zhao, L.; Zhang, F.; Cowling, B. J.; Li, F.; Leung, G. M. Temporal dynamics in viral shedding and transmissibility of COVID-19. *Nat. Med.* **2020**, *26* (5), 672−675.
(19) Sethuraman, N.; Jeremiah, S. S.; Ryo, A. Interpreting Diagnostic Tests for SARS-CoV-2. *JAMA* **2020**, *323* (22), 2249−2251.
(20) Choi, B.; Choudhary, M. C.; Regan, J.; Sparks, J. A.; Padera, R. F.; Qiu, X.; Solomon, I. H.; Kuo, H.-H.; Boucau, J.; Bowman, K.; Adhikari, U. D.; Winkler, M. L.; Mueller, A. A.; Hsu, T. Y. T.; Desjardins, M.; Baden, L. R.; Chan, B. T.; Walker, B. D.; Lichterfeld, M.; Brigl, M.; Kwon, D. S.; Kanjilal, S.; Richardson, E. T.; Jonsson, A. H.; Alter, G.; Barczak, A. K.; Hanage, W. P.; Yu, X. G.; Gaiha, G. D.; Seaman, M. S.; Cernadas, M.; Li, J. Z. Persistence and Evolution of SARS-CoV-2 in an Immunocompromised Host. *New England Journal of Medicine* **2020**, *383* (23), 2291−2293.
(21) Taramasso, L.; Sepulcri, C.; Mikulska, M.; Magnasco, L.; Lai, A.; Bruzzone, B.; Dentone, C.; Bassetti, M. Duration of isolation and precautions in immunocompromised patients with COVID-19. *Journal of Hospital Infection* **2021**, *111*, 202−204.
(22) Aydillo, T.; Gonzalez-Reiche, A. S.; Aslam, S.; van de Guchte, A.; Khan, Z.; Obla, A.; Dutta, J.; van Bakel, H.; Aberg, J.; García-Sastre, A.; Shah, G.; Hohl, T.; Papanicolaou, G.; Perales, M.-A.; Sepkowitz, K.; Babady, N. E.; Kamboj, M. Shedding of Viable SARS-CoV-2 after Immunosuppressive Therapy for Cancer. *New England Journal of Medicine* **2020**, *383* (26), 2586−2588.
(23) van Kampen, J. J. A.; van de Vijver, D. A. M. C.; Fraaij, P. L. A.; Haagmans, B. L.; Lamers, M. M.; Okba, N.; van den Akker, J. P. C.; Endeman, H.; Gommers, D. A. M. P. J.; Cornelissen, J. J.; et al. Duration and key determinants of infectious virus shedding in hospitalized patients with coronavirus disease-2019 (COVID-19). *Nature. Communications* **2021**, *12* (1), 267.
(24) Toptan, T.; Eckermann, L.; Pfeiffer, A. E.; Hoehl, S.; Ciesek, S.; Drosten, C.; Corman, V. M. Evaluation of a SARS-CoV-2 rapid antigen test: Potential to help reduce community spread? *Journal of Clinical Virology* **2021**, *135*, No. 104713.
(25) Mina, M. J.; Peto, T. E.; García-Fiñana, M.; Semple, M. G.; Buchan, I. E. Clarifying the evidence on SARS-CoV-2 antigen rapid tests in public health responses to COVID-19. *Lancet* **2021**, *397* (10283), 1425−1427.
(26) Peeling, R. W.; Olliaro, P. L.; Boeras, D. I.; Fongwen, N. Scaling up COVID-19 rapid antigen tests: promises and challenges. *Lancet. Infectious diseases* **2021**, *21*, e290−e295.
(27) Bullard, J.; Dust, K.; Funk, D.; Strong, J. E.; Alexander, D.; Garnett, L.; Boodman, C.; Bello, A.; Hedley, A.; Schiffman, Z.; Doan, K.; Bastien, N.; Li, Y.; Van Caeseele, P. G.; Poliquin, G. Predicting Infectious Severe Acute Respiratory Syndrome Coronavirus 2 From Diagnostic Samples. *Clin Infect Dis* **2020**, *71* (10), 2663−2666.
(28) La Scola, B.; Le Bideau, M.; Andreani, J.; Hoang, V. T.; Grimaldier, C.; Colson, P.; Gautret, P.; Raoult, D. Viral RNA load as determined by cell culture as a management tool for discharge of SARS-CoV-2 patients from infectious disease wards. *Eur. J. Clin Microbiol Infect Dis* **2020**, *39* (6), 1059−1061.
(29) McKay, S. L.; Tobolowsky, F. A.; Moritz, E. D.; Hatfield, K. M.; Bhatnagar, A.; LaVoie, S. P.; Jackson, D. A.; Lecy, K. D.; Bryant-Genevier, J.; Campbell, D.; Freeman, B.; Gilbert, S. E.; Folster, J. M.; Medrzycki, M.; Shewmaker, P. L.; Bankamp, B.; Radford, K. W.; Anderson, R.; Bowen, M. D.; Negley, J.; Reddy, S. C.; Jernigan, J. A.; Brown, A. C.; McDonald, L. C.; Kutty, P. K. Performance Evaluation of Serial SARS-CoV-2 Rapid Antigen Testing During a Nursing Home Outbreak. *Ann. Int. Med.* **2021**, *174* (7), 945−951.
(30) Pekosz, A.; Parvu, V.; Li, M.; Andrews, J. C.; Manabe, Y. C.; Kodsi, S.; Gary, D. S.; Roger-Dalbert, C.; Leitch, J.; Cooper, C. K. Antigen-Based Testing but Not Real-Time Polymerase Chain Reaction Correlates With Severe Acute Respiratory Syndrome Coronavirus 2 Viral Culture. *Clinical Infectious Diseases* **2021**, *73* (9), e2861−e2866.
(31) Pray, I. W.; Ford, L.; Cole, D.; Lee, C.; Bigouette, J. P.; Abedi, G. R.; Bushman, D.; Delahoy, M. J.; Currie, D.; Cherney, B.; et al. Performance of an Antigen-Based Test for Asymptomatic and Symptomatic SARS-CoV-2 Testing at Two University Campuses - Wisconsin, September-October 2020. *MMWR Morb Mortal Wkly Rep* **2021**, *69* (5152), 1642−1647.
(32) Luan, J.; Seth, A.; Gupta, R.; Wang, Z.; Rathi, P.; Cao, S.; Gholami Derami, H.; Tang, R.; Xu, B.; Achilefu, S.; Morrissey, J. J.; Singamaneni, S. Ultrabright fluorescent nanoscale labels for the femtomolar detection of analytes with standard bioassays. *Nat. Biomed Eng.* **2020**, *4* (5), 518−530.
(33) Liang, C.; Luan, J.; Wang, Z.; Jiang, Q.; Gupta, R.; Cao, S.; Liu, K.-K.; Morrissey, J. J.; Kharasch, E. D.; Naik, R. R.; Singamaneni, S. Gold Nanorod Size-Dependent Fluorescence Enhancement for Ultrasensitive Fluoroimmunoassays. *ACS Appl. Mater. Interfaces* **2021**, *13* (9), 11414−11423.
(34) Wang, Z.; Luan, J.; Seth, A.; Liu, L.; You, M.; Gupta, P.; Rathi, P.; Wang, Y.; Cao, S.; Jiang, Q.; Zhang, X.; Gupta, R.; Zhou, Q.; Morrissey, J. J.; Scheller, E. L.; Rudra, J. S.; Singamaneni, S. Microneedle patch for the ultrasensitive quantification of protein biomarkers in interstitial fluid. *Nature Biomedical Engineering* **2021**, *5* (1), 64−76.
(35) Gupta, R.; Gupta, P.; Wang, S.; Melnykov, A.; Jiang, Q.; Seth, A.; Wang, Z.; Morrissey, J. J.; George, I.; Gandra, S.; Sinha, P.; Storch, G. A.; Parikh, B. A.; Genin, G. M.; Singamaneni, S. Ultrasensitive lateral-flow assays via plasmonically active antibody-conjugated fluorescent nanoparticles. *Nature Biomedical Engineering* **2023**, DOI: 10.1038/s41551-022-01001-1.
(36) Zhao, W.; Ali, M. M.; Brook, M. A.; Li, Y. Rolling Circle Amplification: Applications in Nanotechnology and Biodetection with Functional Nucleic Acids. *Angew. Chem., Int. Ed.* **2008**, *47* (34), 6330−6337.
(37) Bruhn, B.; Qejvanaj, F.; Gregorkiewicz, T.; Linnros, J. Temporal correlation of blinking events in CdSe/ZnS and Si/SiO2 nanocrystals. *Physica B: Condensed Matter* **2014**, *453*, 63−67.
(38) Young, S.; Taylor, S. N.; Cammarata, C. L.; Varnado, K. G.; Roger-Dalbert, C.; Montano, A.; Griego-Fullbright, C.; Burgard, C.; Fernandez, C.; Eckert, K.; et al. Clinical Evaluation of BD Veritor SARS-CoV-2 Point-of-Care Test Performance Compared to PCR-Based Testing and versus the Sofia 2 SARS Antigen Point-of-Care Test. *J. Clin. Microbiol.* **2020**, *59* (1), DOI: 10.1128/JCM.02338-20.
(39) Tan, S. S.; Chew, K. L.; Saw, S.; Jureen, R.; Sethi, S. Cross-reactivity of SARS-CoV-2 with HIV chemiluminescent assay leading to false-positive results. *Journal of Clinical Pathology* **2021**, *74* (9), 614.
(40) Grobben, M.; van der Straten, K.; Brouwer, P. J. M.; Brinkkemper, M.; Maisonnasse, P.; Dereuddre-Bosquet, N.; Appelman, B.; Lavell, A. H. A.; van Vught, L. A.; Burger, J. A.; et al. Cross-reactive antibodies after SARS-CoV-2 infection and vaccination. *eLife* **2021**, *10*, No. e70330.
(41) Galipeau, Y.; Siragam, V.; Laroche, G.; Marion, E.; Greig, M.; McGuinty, M.; Booth, R. A.; Durocher, Y.; Cuperlovic-Culf, M.; Bennett, S. A. L.; Crawley, A. M.; Giguère, P. M.; Cooper, C.; Langlois, M.-A. Relative Ratios of Human Seasonal Coronavirus Antibodies Predict the Efficiency of Cross-Neutralization of SARS-CoV-2 Spike Binding to ACE2. *eBioMedicine* **2021**, *74*, No. 103700.
(42) Weekly epidemiological update on COVID-19 - 8 June 2021. World Health Organization.https://www.who.int/publications/m/item/weekly-epidemiological-update-on-covid-19---8-june-2021 (accessed 2023/12/08).
(43) Implication of variants on COVID-19 antigen test detection. PATH.https://www.path.org/programs/diagnostics/covid-dashboard-implication-variants-covid-19-antigen-test-detection/ (accessed 2023-12-08).
(44) Bourassa, L.; Perchetti, G. A.; Phung, Q.; Lin, M. J.; Mills, M. G.; Roychoudhury, P.; Harmon, K. G.; Reed, J. C.; Greninger, A. L. A SARS-CoV-2 Nucleocapsid Variant that Affects Antigen Test Performance. *Journal of Clinical Virology* **2021**, *141*, No. 104900.
(45) Vecchio, C. D.; Brancaccio, G.; Brazzale, A. R.; Lavezzo, E.; Onelia, F.; Franchin, E.; Manuto, L.; Bianca, F.; Cianci, V.; Cattelan,

A.; Toppo, S.; Crisanti, A. Emergence of N antigen SARS-CoV-2 genetic variants escaping detection of antigenic tests. *medRxiv*, 2021, 2021.03.25.21253802 (accessed 2023-12-11).

(46) Galloway, S. E.; Paul, P.; MacCannell, D. R.; Johansson, M. A.; Brooks, J. T.; MacNeil, A.; Slayton, R. B.; Tong, S.; Silk, B. J.; Armstrong, G. L.; Biggerstaff, M.; Dugan, V. G. Emergence of SARS-CoV-2 B.1.1.7 Lineage - United States, December 29, 2020-January 12, 2021. *MMWR. Morbidity and mortality weekly report* **2021**, *70* (3), 95−99.

(47) Singh, J.; Samal, J.; Kumar, V.; Sharma, J.; Agrawal, U.; Ehtesham, N. Z.; Sundar, D.; Rahman, S. A.; Hira, S.; Hasnain, S. E. Structure-Function Analyses of New SARS-CoV-2 Variants B.1.1.7, B.1.351 and B.1.1.28.1: Clinical, Diagnostic, Therapeutic and Public Health Implications. *Viruses* **2021**, *13* (3), 439.

https://doi.org/10.1021/acs.nanolett.3c03789
Nano Lett. 2024, 24, 229−237